Modeling oxygen mass transfer in surfactant solutions considering hydrodynamics and physico-chemical phenomena

Gaëlle Lebrun, Nathalie Clergerie, Gilles Hébrard, Nicolas Dietrich

Modeling oxygen mass transfer in surfactant solutions considering hydrodynamics and physico-chemical phenomena

Gaëlle Lebrun[1], Nathalie Clergerie[1], Gilles Hébrard[1], Nicolas Dietrich[1,*]

[1] *Toulouse Biotechnology Institute (TBI), Université de Toulouse, CNRS, INRAE, INSA, Toulouse, France*

*Corresponding author(s): dietrich@insa-toulouse.fr

Abstract

The present study offers a predictive correlation for oxygen transfer based on the exhaustive analysis of more than 300 isolated gas bubbles and the examination of interfacial colonization phenomena occurring in the presence of surfactants. The correlation is formulated by accounting for two key aspects: the hydrodynamic influence exerted by surfactants on mass transfer and the physico-chemical hindrance caused by surfactant adsorption. While the correlation holds substantial promise for application in wastewater treatment facilities, it has hitherto been exclusively employed for bubbles with an equivalent diameter (d_b) smaller than 1.5 mm and in systems featuring a singular surfactant species in the liquid phase. With a view to harnessing a model for its integration into wastewater treatment plants, our study endeavors to elucidate the methodology for expanding the applicability of the correlation to bubbles with higher Reynolds numbers (d_b > 1.5 mm). To this end, the study leverages the work of Sardeing et al. (2006) and demonstrates its effectiveness in scenarios typified by the coexistence of multiple surfactant species, which is representative of common constituents in wastewater treatment plant environments.

Keywords: bubble column; surfactants; liquid-side mass transfer coefficient; correlation; model

Introduction

Processes that involve gas–liquid mass transfer are found in numerous industries, such as medicine, environment, and food. However, modeling mass transfer is a challenge when the liquid phase contains impurities. Such is the case of wastewater treatment plants, where oxygen transfer is necessary to keep microorganisms responsible for pollutant biodegradation alive. Oxygen transfer in aerated sludge tanks is performed in liquids containing surfactants and in which the rheology is slightly shear thinning (Quintero,

2015). Due to the complex liquid phase, predicting oxygen transfer to provide adequate aeration for the microorganisms remains difficult; yet, it is necessary for good process design (Gillot et al., 2005). Previous studies have led to understand mass transfer in a bubble column containing a complex liquid phase. The first mechanism involved in mass transfer in the presence of contaminants is based on hydrodynamic modifications. Contaminants decrease the velocity of a bubble rising in a liquid until it reaches one of the solid spheres, with the resulting mass transfer being impacted due to the substantial decrease of surface renewal (Alves et al., 2005; Clift et al., 1978; Rosso et al., 2006; Takemura, 2005; Weber, 1975). The resulting mass transfer depends on the surface covered by surfactants, which can be calculated from its drag coefficient, and ranges between that of a clean bubble and a fully contaminated bubble (Sadhal and Johnson, 1983). Some studies have identified an additional "barrier effect" resulting from the presence of surfactants (Hebrard, Zeng, and Loubière, 2009; Jimenez et al., 2014; Lebrun et al., 2021), while others have highlighted that the structure of the surfactants—highly related to its adsorption properties—plays an important role in mass transfer decrease (Chen et al., 2013; García-Abuín et al., 2010; Jia et al., 2015; Lebrun et al., 2022a; Orhan and Dursun, 2016; Rosso et al., 2006; Sardeing et al., 2006).

More recently, Direct Numerical Simulation (DNS) approaches have been used by various authors (Dani et al., 2022; Deising et al., 2018; Kentheswaran et al., 2022; Pesci et al., 2018; Weiner et al., 2019) to physically explain the surfactant reduction on the gas–liquid mass transfer coefficient. This numerical simulation considers a surfactant adsorption constant.

The aforementioned studies highlight the necessity to consider both bubble hydrodynamics and its physico-chemical properties to build a reliable and predictive mass transfer model.

The present paper brings together a set of results from our previous papers (Lebrun et al., 2022a, 2022b; Sardeing et al., 2006), which studied the effect of surfactants on the liquid-side mass transfer coefficient. Our dataset contains both accurate information on bubble hydrodynamic conditions and surfactant adsorption properties, linked to the measured values of the liquid-side mass transfer coefficient. The collected data are used to test and improve the model introduced in Lebrun et al. (2022b), where the Sherwood number is predicted as a function of hydrodynamic and physico-chemical parameters. For the first time, the proposed relationship is tried and assessed for a mixture of surfactants.

Materials and methods

Most of the experimental results present in this paper were obtained using the materials and methods

reported in Lebrun et al., 2022a. Planar Laser-Induced Fluorescence with Inhibition (PLIFI) was implemented in a column (0.1×0.1×0.3 m^3) filled with 2 L of aqueous solution with various surfactant types to be tested (Figure 1). Millimetric single air bubbles were generated in the solution using a needle (⌀ = 75 μm) connected to a syringe pump (DPC Intelligent Mass Flow Controller, Aalborg, USA) which can flow 0–100 mL/min of compressed air. A Photon SA3 camera (8 bits, 2000 fps, 1024×1024 pixels) was used to record the bubble rise through the column at a rate of 250 images·s^{-1} in a window of 1920x500 $pixels^2$ (Figure 1). Using this experimental setup and homemade MATLAB® software, we were able to conduct contour analysis through the binarization of the bubble images, allowing us to calculate bubble diameter, eccentricity and velocity. The amount of oxygen transferred in the bubble wake during its ascension through the column was measured by fluorescence inhibition of a ruthenium complex, selected in accordance with the charge of the surfactant under test (Lebrun et al., 2022a, 2022b). A conventional ruthenium complex (CAS: 20782-45-7, Sigma-Aldrich, USA) was used when cationic surfactants were under test and $[Ru(dpp\text{-}diSO_3)_3]Na_4$ when anionic surfactants were present. The fluorophore was excited at 532 nm with a horizontal laser sheet placed on a plane perpendicular to the bubble wake, 50 mm above the injection point of the bubble. Fluorescence intensity emission was recorded using a CCD camera synchronized with the laser frequency and focused on the laser sheet. The camera was placed below the column to observe the evolution of the spot emission due to inhibition of fluorescence by oxygen presence. We used an optical oxygen probe (HACH HQd Portable Meter + IntelliCAL LDO Probe) and fluorescence intensity emissions obtained under well-known oxygen concentration solutions to build a Stern–Volmer calibration curve, thus stablishing a link between pixel intensity and oxygen concentration. The flux of oxygen transferred by the rising bubble into a surfactant solution was then determined from the bubble velocity times the integral of the oxygen spot at the bubble wake obtained by the PLIFI method, as noted in equation (1). The liquid-side mass transfer coefficient kl can be calculated from the measured flux, the driving force and the bubble surface.

$$F_{O_2} = V_b \iint [O_2](x,y)dxdy = k_L S_b([O_2]^* - [O_2]) \quad (1)$$

Different experiments were conducted with various surfactants found in wastewater treatment tanks. All solutions were prepared using ultra-pure water with a conductivity of 0.054 mS·cm^{-1}. The surfactants chosen to study their effect on oxygen transfer were sodium dodecylbenzenesulfonate (SDBS, CAS: 25155-30-0, Sigma Aldrich), sodium dodecyl sulfate (SDS, CAS: 151-21-3, Sigma Aldrich) and Triton X-100

64 (TX100, CAS: 9036-19-5, Sigma Aldrich).

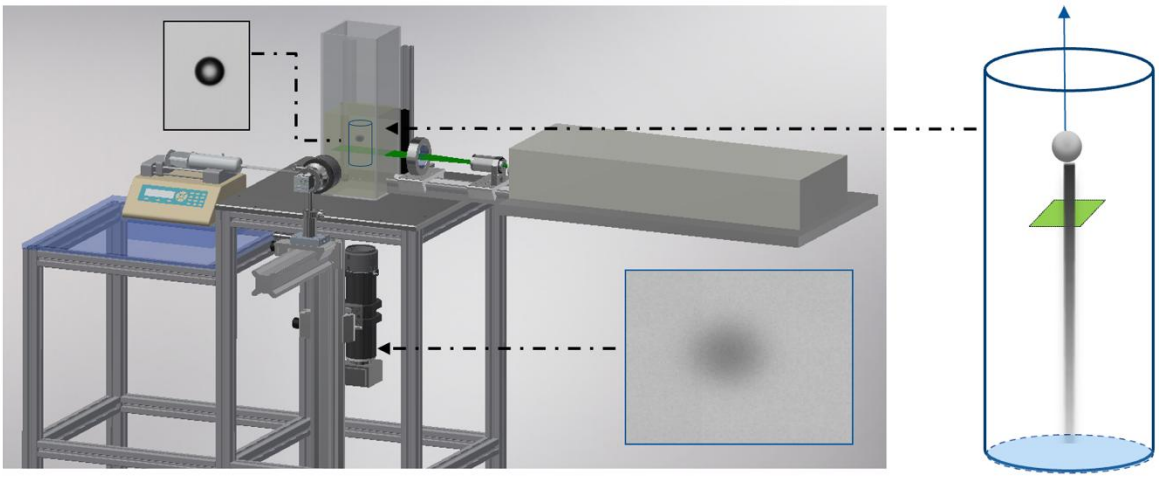

65

66 Figure 1. Experimental setup.

67 Surfactant solutions were prepared at concentrations between $1.3x10^{-3}$ and $2.5x10^{-7}$ mol/L^{-1}. The surface
68 tension of solutions was measured according to the Du Noüy ring method (K6 tensiometer, Krüss,
69 Germany) and assumed that equilibrium was reached after one hour.

70 As the dataset used to assess the proposed modeling encompasses different studies, we report all relevant
71 information required to identify the conditions under test in Table 1.

72 Table 1. Experimental parameters

Bubble diameter (mm)	Fluid properties	Surfactant & concentration	Method	Reference paper
$0.82 < d_b < 1.08$	Water solution	**Non ionic surfactant** Triton X-100 (TX100, CAS: 9002-93-1, Sigma Aldrich, USA), Triton X-102 (TX102, CAS: 9036-19-5, Sigma Aldrich, USA) and Triton X-165 (TX165, CAS: 9636-19-5, Sigma Aldrich, USA) and TX305 (CAS: 9002-93-1, Sigma Aldrich, USA). $2.5x10^{-8}$ mol/L to $5x10^{-3}$ mol/L	PLIFI with ruthenium complex (CAS: 20782-45-7, Sigma-Aldrich, USA)	(Lebrun et al.2021)
$0.82 < d_b < 1.08$	Water solution	**Cationic surfactant** CH3(CH2)nN(CH3)3Cl With n = 7, 11 or 15 $2.5x10^{-8}$ to $5x10^{-3}$ mol/L	PLIFI with ruthenium complex (CAS: 20782-45-7, Sigma-Aldrich, USA)	(Lebrun et al., 2022a)

$0.9 < d_b < 1.3$	Water solution	**Anionic surfactant** Dodecyl sulfate sodium salt (SDS, CAS: 151-21-3, Sigma-Aldrich, USA) and tetradecyl sulfate sodium salt (STS, CAS: 1191-50-0, Sigma-Aldrich, USA) $2.5x10^{-7}$ to $1.3x10^{-3}$ mol/L	PLIFI with ruthenium complex $[Ru(dpp\text{-}diSO_3)_3]Na_4$	(Lebrun et al., 2022b)
$1.5 < d_b < 7$	Water solution	**Anionic surfactant** Sodium laurylsulfate $1.3x10^{-4}$ to $4.97x10^{-3}$ mol/L **Cationic surfactant** Lauryl dimethyl benzyl ammonium bromine $2.75x10^{-4}$ to $5x10^{-3}$ mol/L **Non-ionic surfactant** Fatty alcohol C12/18, 10 EO, n-butyl end-capped $1.23x10^{-4}$ to $5x10^{-3}$ mol/L	Glass bubble column ($\varnothing$ = 0.05 m) with a liquid height of 0.25 m. Mass balance on sulfite sodium (Na_2SO_3) concentration during aeration time for volumetric mass transfer coefficient determination; de-oxygenation made using nitrogen injection	(Sardeing et al., 2006) (Sardeing et al., 2006)

Modeling

The originality of the proposed model lies in its consideration of hydrodynamics and surfactant effects into a single relationship containing the $\theta_{cap(°)}$ model for hydrodynamic effects and Frumkin adsorption parameters for surfactant effects. This new model is an improved version of that of Lebrun et al. (2022b), extending its applicability to larger bubble diameters and surfactant mixtures.

The physical model proposed by Lebrun et al. (2022b) considers hydrodynamic parameters and surfactant adsorption on the bubble.

Surfactant hydrodynamic effects:

The effect of surfactants on bubble hydrodynamics implies that, when the surfactants are adsorbed at the interface of the bubble, the interface can be deemed as rigid and the velocity at the interface is thus zero. The thickness of the boundary layer is that of a solid sphere(Clift et al., 1978), with the resulting Sherwood number being described in equation (2):

$$Sh_{contaminated} = Re^{0.5}Sc^{0.33} \quad (2)$$

On the contrary, if the bubble is free of surfactants, the slip condition is satisfied; the resulting Sherwood number is modeled in equation (3):

$$Sh_{clean} = Re^{0.5} Sc^{0.5} \qquad (3)$$

Since the bubble may not be fully contaminated by surfactants, the latter are swept toward the rear of the bubble and form a cap where surfactant surface concentration is high. At the nose of the bubble, surfactant surface concentration is near zero (Palaparthi et al., 2006). The cap angle is calculated by the correlation (Sadhal and Johnson, 1983) shown in equation (4):

$$C_D^* = \frac{C_D - C_D^m}{C_D^{im} - C_D^m} = \frac{1}{2\pi}\left(2\left(\pi - \theta_{cap}\right) + \sin\left(\theta_{cap}\right) + \sin\left(2\theta_{cap}\right) - \frac{1}{3}\sin\left(3\theta_{cap}\right)\right) \qquad (4)$$

Where C_D^* is the normalized drag coefficient, θ_{cap} is the cap angle (rad), C_D is the measured drag coefficient (equation (5)) and C_D^{im} and C_D^m the immobile and mobile coefficients. In the case of bubbles with $d_b < 1.5$ mm, these are determined using Schiller and Naumann (1933) and Mei et al. (1994) correlations respectively, as shown in equations (6) and (7):

$$C_D = \frac{4}{3}\frac{(\rho_L - \rho_G) g d_{eq}}{\rho_L V_b^2} \qquad (5)$$

$$C_D^{im} = \frac{24}{Re}(1 + 015 Re^{0.687}) \qquad (6)$$

$$C_D^m = \frac{16}{Re}\left(1 + \frac{Re}{8 + 0.5(Re + 3.315 Re^{0.5})}\right) \qquad (7)$$

The ratio covered by a surfactant can then be described as R_{cap}, as shown in equation (8):

$$R_{cap} = \frac{180 - \theta_{cap(°)}}{180} \qquad (8)$$

This overlap is theoretical, deduced from the experimental Reynolds number of the bubble. We can compare the R_{cap} overlap with the chemical overlap ($\theta = \Gamma/\Gamma\infty$) deduced from plotting surface tension against concentration. While the θ overlap yields the value of equilibrium overlap from a physico-chemical point of view (by means of the isotherms obtained from Langmuir 1917 and Frumkin 1925), the R_{cap} overlap represents a real overlap calculated from the effect of surfactants on bubble velocity. Neither overlap is more significant than the other; they merely represent similar effects but different equilibrium

conditions. As for the θ overlap, it is possible that equilibrium is not reached at the time of measurement, which occurs around 0.25 s after the creation of the interface. Since surfactant contamination of the bubble occurs within the first few seconds—according to the dynamic surface tension data—there is a significant effect of the presence of surfactants, even if they have yet to reach their equilibrium concentrations at the interface.

Surfactant physico-chemical effects:

The influence of the surfactant on bubble hydrodynamics makes the averaged mass transfer oscillate between $Sh_{contaminated}$ and Sh_{clean}, balanced by $R_{cap.}$ However, as highlighted by (Lebrun et al., 2022b), the presence of surfactant results in an additional barrier effect to mass transfer. This additional effect can be modeled with the concentration of surfactant in the bulk (C, $mol \cdot m^{-3}$), the adsorption constant of the surfactant (K, $m^3 \cdot mol^{-1}$) and the electrostatic interactions between monomers (a_F, unitless), as described in Figure 2. These parameters are determined by the isotherm for uncharged (Langmuir, 1917) or charged surfactants (Frumkin, 1925).

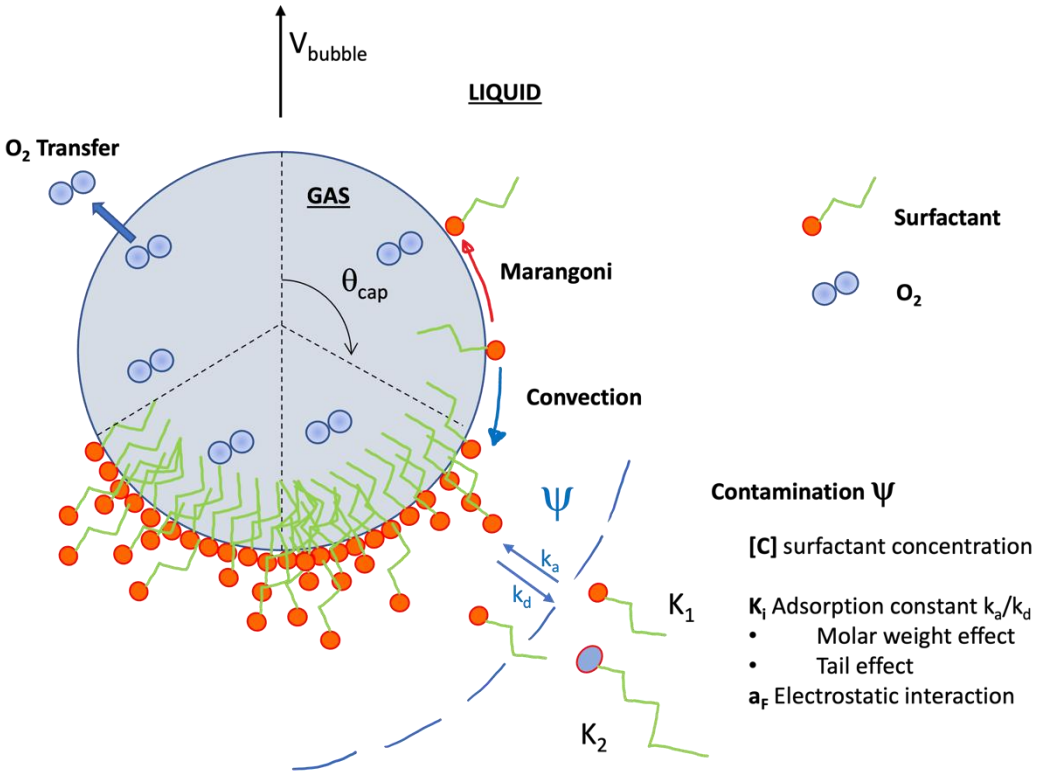

Figure 2. Marangoni, convection, and contamination effects on oxygen mass transfer in the presence of

surfactants.

Langmuir isotherm

The Langmuir isotherm (1917) is the most used in the field. Langmuir considers the monomolecular layer of adsorbed molecules as being subject to the dynamic equilibrium between molecules arriving at and leaving the surface. Each molecule occupies an adsorption site. Langmuir makes the following assumptions: (a) the rate of adsorption is proportional to the fraction of sites unoccupied by the solute and proportional to the solute concentration of the liquid phase, and (b) the rate of desorption is proportional to the fraction of sites occupied. The total flux of surfactants j_s ($mol \cdot m^{-2} \cdot s^{-1}$) adsorbed at the interface over time results from a flux of surfactants adsorbed according to adsorption constant k_a ($m^3 \cdot mol^{-1} \cdot s^{-1}$), minus a flux of surfactants desorbed according to a desorption constant k_d (s^{-1}):

$$j_s = k_a C_i(\Gamma_\infty - \Gamma) - k_d \Gamma \qquad (9)$$

Where Γ_∞ ($mol.m^{-2}$) is the maximum surface concentration of surfactant at given temperature and pressure conditions. By definition, the flux of adsorbed surfactants at equilibrium is equal to the flux of desorbed surfactants, so we can consider that $j_s=0$; we then obtain:

$$\Gamma_i = \frac{\Gamma_\infty K_{LM} C_i}{1+K_{LM} C_i} \qquad (10)$$

Where K_{LM} is the Langmuir constant generally expressed in $m^3 \cdot mol^{-1}$ and is equal to the ratio of adsorption and desorption constants ($K_{LM} = \frac{k_a}{k_d}$). Since $\theta = \frac{\Gamma_i}{\Gamma_\infty}$, equation (10) can be written as follows:

$$K_{LM} C_i = \frac{\theta}{1-\theta} \qquad (11)$$

According to Gibbs (1874), plotting surface tension versus surfactant concentration gives a linear relationship existing between slope of this curve and surface concentration:

$$\Gamma_i = \frac{-C_i.d\gamma}{n_G.R.T.dC} \qquad (12)$$

With $n_G = 1$ for no ionic surfactant and $n_G = 2$ for ionic surfactant

By integrating equation (10) and combining it with equation (11) and then with equation (12), we obtain an equation of state that directly links surface tension γ and concentration, as expressed in equation (13):

$$\gamma = \gamma_0 + n_G R.T.\Gamma_\infty[\ln(1-\theta)] \quad (13)$$

Where γ_0 is the surface tension of the solvent without surfactant ($N \cdot m^{-1}$).

Frumkin isotherm

The Frumkin isotherm (1925) is based on the approach of Langmuir while considering possible electrostatic interactions between monomers. The equation described by Langmuir's model (equation 11) then becomes equation (14):

$$K_F C_i = \frac{\theta}{(1-\theta)} \exp(-2a_F.\theta) \quad (14)$$

The equation of state (13) thus becomes equation (15):

$$\gamma = \gamma_0 + n_G.R.T.\Gamma_\infty[\ln(1-\theta) + a_F.\theta^2] \quad (15)$$

K_F is Frumkin's constant and is generally expressed in $m^3 \cdot mol^{-1}$. The constant a_F (unitless) is added to account for electrostatic interactions. Although the Frumkin isotherm takes into account interactions between monomers, the system is complex and there is no analytical solution of γ = f(Ci). Therefore, a numerical resolution is required to obtain this type of isotherm.

In order to determine the parameters of these equations, we used the "SA" simulation and adjustment software — a free, open-source software package developed by the Laboratory of Chemistry of Colloids, Polymers & Complex Assemblies (Softmat/UMR-CNRS 5623/Université Paul Sabatier) in Toulouse. The software simulates model behavior as a function of an independent variable (in our case, concentration) and adjusts its parameters on the basis of experimental data. The software relies on a method of adjustment by integration using least squares to calculate the error, with variable adjustment based on Powell's method (Powell, 1964). While the program is specifically built for the Frumkin model, it can be easily adapted to the Langmuir model by fixing $a_F = 0$.

Global model:

By considering all these parameters, the resulting averaged Sherwood number around the bubble can be expressed as follows:

$$Sh_{correlated} = \left(\left(1 - R_{cap}\right)Sh_{clean} + R_{cap}Sh_{contaminated}\right)\left(\frac{K \cdot C}{e^{-2a_F\theta}}\right)^{\psi} \qquad (16)$$

Where ψ is a coefficient that needs to be determined and is a function of the ratio between the convection force and adsorption flux that exist at the bubble interface, which can depend on bubble size and shape.

Results and discussion

Using our dataset (Sardeing et al., 2006; Lebrun et al., 2022a, 2022b), which includes accurate information on bubble hydrodynamic conditions and surfactant adsorption properties along with the measured values of the liquid-side mass transfer coefficient k_L, we tested and improved the model introduced in Lebrun et al. (2022b) where the Sherwood number is predicted as a function of hydrodynamic and physico-chemical parameters for three ranges of bubble diameters (d_b < 1.5 mm; 1.5 < d_b < 3.5 mm; and d_b > 3.5 mm).

Bubbles with d_b < 1.5 mm

Lebrun et al. (2022b) highlighted that the Sherwood number of small bubbles can be modeled using equation (8). In this case, the value of ψ depends on the balance between advection force—which sweeps surfactants toward the rear of the bubble—and the adsorption flux of surfactants (equation (17)) that moves faster from the bulk interface.

$$\psi = f\left(\frac{convection}{contamination}\right) \qquad (17)$$

In Lebrun et al. (2022b), the balance between convection and contamination was expressed using the Reynolds number Re, adsorption constant K, coverage ratio θ, constant a_F, and bulk concentration C. The value of ψ is expressed in equation (18):

$$\psi = f\left(\frac{e^{-2 \cdot a_F \cdot \theta \cdot Re}}{K \cdot C}\right) \qquad (18)$$

For bubbles lower than 1.5 mm, operating conditions were separated into six, in function of their value of $\frac{e^{-2 \cdot a_F \cdot \theta \cdot Re}}{K \cdot C}$. A value of ψ was determined for all six conditions; the standard deviation between the

experimental results and the results predicted by the correlation was 24%. Instead of only determining a value of ψ for a range of operating conditions, we can also determine if the function expressed in equation (18) can be modeled. In Figure 3, a value of ψ was determined for each experimental point to fit the experimental and correlation values.

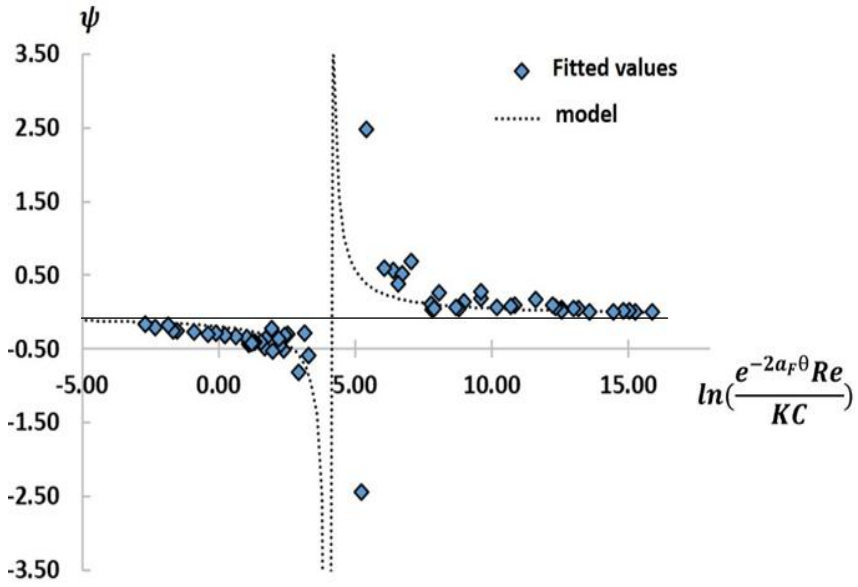

Figure 3. Fitted values of the factor ψ in function of the ratio between convection and contamination.

The variation of ψ along with the convection–contamination ratio (i.e. $\frac{e^{-2a_F\theta}Re}{KC}$) can be modeled using the function shown in equation (19):

$$\psi = \alpha + \frac{\beta}{\ln\left(\frac{e^{-2a_F\theta}Re}{KC}\right)+\varepsilon} \qquad (19)$$

Where α, β and ε are constants equal to -0.047, 0.59 and -4.04, respectively, after fitting the experimental points with equation (19) using the least squares method. The fitted curve is shown as a dotted line in Figure 3. The factor ψ can then be estimated through the correlation expressed in equation (20):

$$\psi = -0.047 + \frac{0.59}{\ln\left(\frac{e^{-2a_F\theta}Re}{KC}\right)-4.04} \qquad (20)$$

If model (16) is applied to the experimental points of Lebrun et al. (2022b), with ψ being determined using equation (20), we observe a mean standard deviation of 30%. Experimental and correlation points are compared in Figure 4. It should be noted that equation (20) results in a critical value when $\ln\left(\frac{e^{-2a_F\theta}Re}{KC}\right) =$

4.04. Should the experimental points approach this critical value, the value of ψ will display a very high sensitivity to Re, K, C and a_F that can increase the error on the predicted Sherwood number.

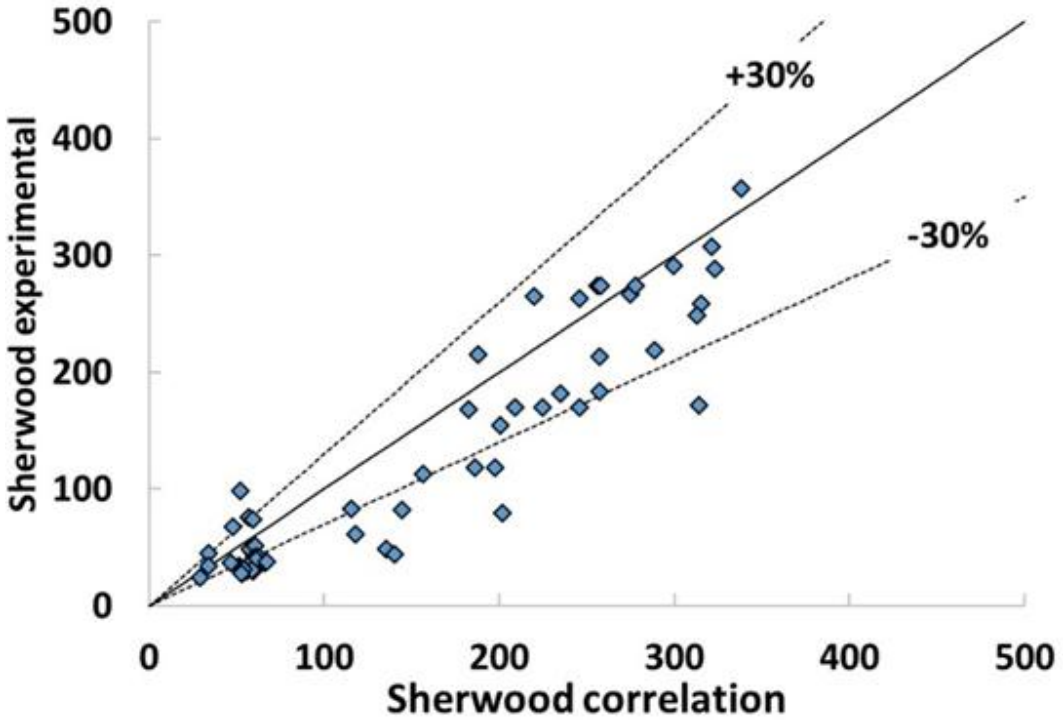

Figure 4. Comparison between experimental Sherwood numbers and those predicted by correlation (8), with a modeled value of ψ.

Bubbles with $d_b > 1.5$ mm (two ranges: $1.5 < d_b < 3.5$ mm and $d_b > 3.5$ mm)

For bubbles with $d_b > 1.5$ mm, we compared the experimental results of Sardeing et al. (2006)— which deal with oxygen transfer in a bubble column in the presence of anionic (sodium lauryl sulfate), nonionic (fatty alcohol $C_{12/18}EO_{10}$) and cationic (Lauryl dimethyl benzyl ammonium bromine) surfactants—with the results predicted by the model.

For bubbles of such size, correlations (6) and (7)—used to calculate C_D^{im} and C_D^{m} respectively—are no longer valid; thus, we must use correlations adapted to this higher diameter. Here, we chose to calculate C_D^{im} from the correlation of (Tomiyama et al., 2002). According to the authors, a fully contaminated bubble rises at a terminal velocity that can be calculated using equation (21):

$$V_b^{im} = \frac{\sin^{-1}\sqrt{1-E^2}-E\sqrt{1-E^2}}{1-E}\sqrt{\frac{8\sigma}{\rho_L}E^{\frac{4}{3}}+\frac{\Delta\rho g d_b}{2\rho_L}\frac{E^{\frac{2}{3}}}{1-E^2}} \qquad (21)$$

Where E is the inverse of the bubble eccentricity (E = 1/X = big axis / little axis). From the terminal velocity V_b^{im}, the corresponding drag coefficient is calculated from equation (4). The clean drag coefficient $C_D{}^m$ was calculated from the Moore equation (Moore, 1965), as shown in equations (22) and (23):

$$C_D^m = \frac{48G(X)}{Re}\left(1 + \frac{H(X)}{Re^{0.5}} + O(Re^{-0.5})\right) \qquad (22)$$

With:

$$G(X) = \frac{1}{3}X^{\frac{4}{3}}(X^2-1)^{\frac{3}{2}}\frac{\left[(X^2-1)^{\frac{1}{2}} - (2-X^2)\sec^{-1}(X)\right]}{\left[X^2\sec^{-1}(X) - (X^2-1)^{\frac{1}{2}}\right]^2} \qquad (23)$$

While H(X) is obtained by numerical integration (see (Moore, 1965)), it can be estimated using linear interpolation; a table of values of H(X) is given in (Moore, 1965) for $1 \leq X \leq 4$. It should be noted that all isotherms plotted in Sardeing et al. (2006) stem from a Langmuir isotherm. As a result, the term that considers electrostatic interaction is neglected.

Bubbles with d_b > 3.5 mm

We consider that convection is strong and always predominant in the case of bubbles with large diameters. As a result, comparing convection and contamination to determine the value of ψ does not make sense. In this instance, only one value of ψ is fitted in equation (16) for all experimental results. The diameter range varies between 3.5 and 5.5 mm; according to the Frumkin isotherm, the coverage ratio θ by surfactant varies between 0.4 and 1.

The value of ψ was fitted to -0.14 using 85 different experimental points under different experimental conditions. Equation (16) then becomes:

$$Sh_{correlated} = \left(\left(1 - R_{cap}\right)Sh_{clean} + R_{cap}Sh_{contaminated}\right)\left(\frac{KC}{e^{-2a_F\theta}}\right)^{-0.14} \qquad (24)$$

Using this equation, the averaged standard deviation between experimental and model values is 12%. The comparison between experimental Sherwood numbers and those obtained through correlation is presented in Figure 5.

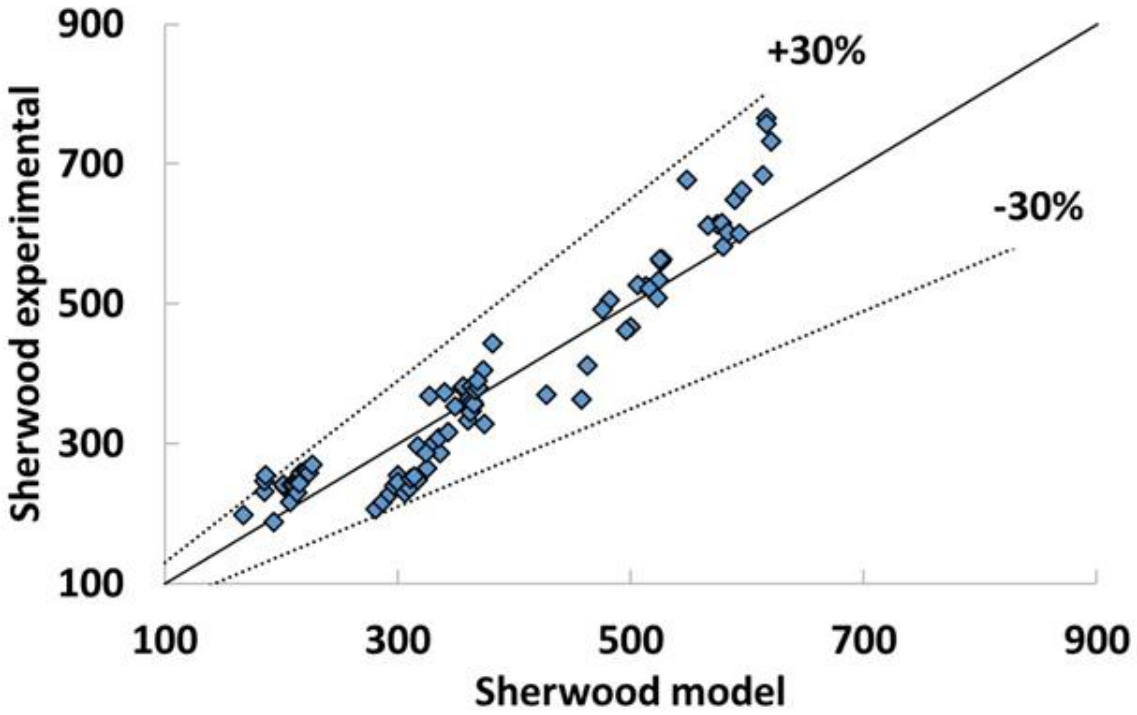

Figure 5. Comparison between experimental Sherwood numbers and those predicted by correlation (16).

Bubbles with 1.5 > d_b > 3.5 mm

The intermediate type concerns bubbles with diameters between 1.5 and 3.5 mm. In Figure 6(a), correlation (16) has been applied to the experimental results of Sardeing et al. (2006). We used the correlation of Tomiyama et al. (2002) and Moore (1965) to determine velocity to estimate the cap angle in this case, while ψ is determined using equation (20). Figure 6(b) compares the experimental results of Sardeing et al. (2006) with correlation (24). These two graphs show that any of the correlations are acceptable to predict the Sherwood number in the presence of surfactants when the bubble diameter lies between 1.5 and 3.5 mm.

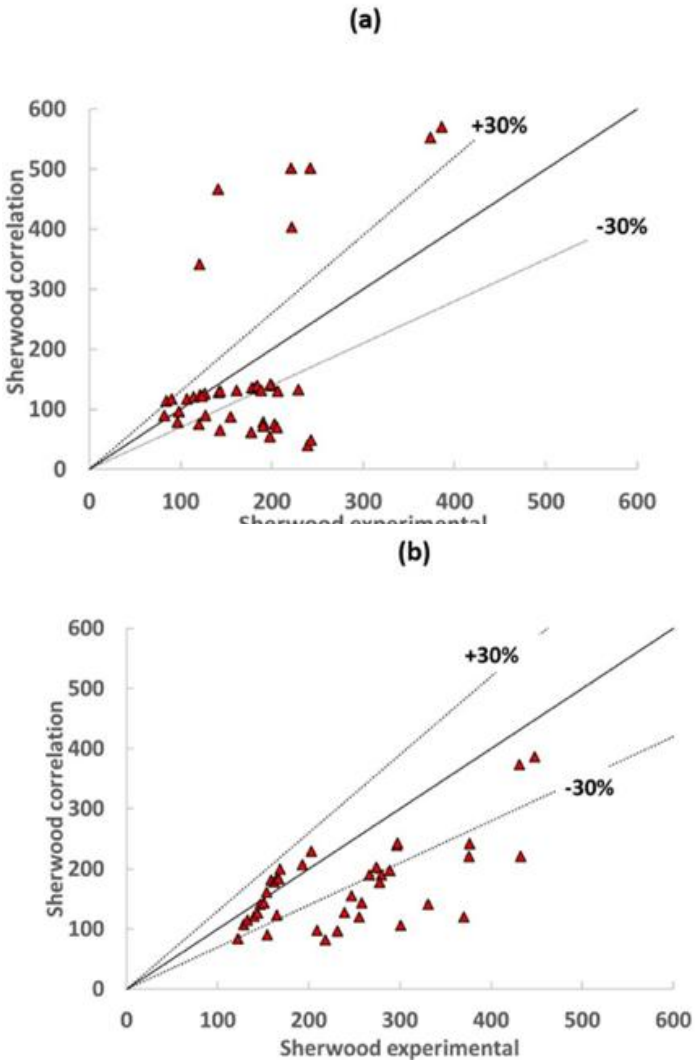

Figure 6. Comparison between experimental Sherwood numbers and those predicted by (a) correlation (16), (b) correlation (24).

A plausible explanation for the difficulty in modeling Sherwood numbers for bubbles where $1.5 > d_b > 3.5$ mm is that, for these diameters, mass transfer is very sensitive to the adsorption of surfactants at the interface. In Sardeing et al. (2006), all isotherms were modelled by Langmuir and the results do not take in account electrostatic interactions, as is the case of Lebrun et al. (2022b) for bubbles where $d_b < 1.5$ mm. It is possible that, if such interactions were to be considered here, the model would better fit the experimental points. More experimental data are required to model oxygen transfer for bubbles of these intermediate diameters.

The correlation is applicable to bubbles of larger size ($d_b > 3.5$ mm). In order to be used in industrial applications, such as wastewater treatment plants, its applicability in liquid phases containing a mix of

surfactants must be verified.

Mix of surfactants and rheology

As a perspective study,

First, we must ensure that the Frumkin model is applicable to the mix of surfactants and that the curve γ=f(concentration) obtained for this type of aqueous phase displays a standard shape. We worked with a mix featuring a molar ratio of 0.33 for each surfactant. Concentration C represents the total concentration of surfactant in the liquid phase (the sum of all surfactants).

The curve of surface tension as a function of the concentration is presented in Figure 7. The dotted line represents the Frumkin model fitted with the "SA" software (SA Software, n.d).

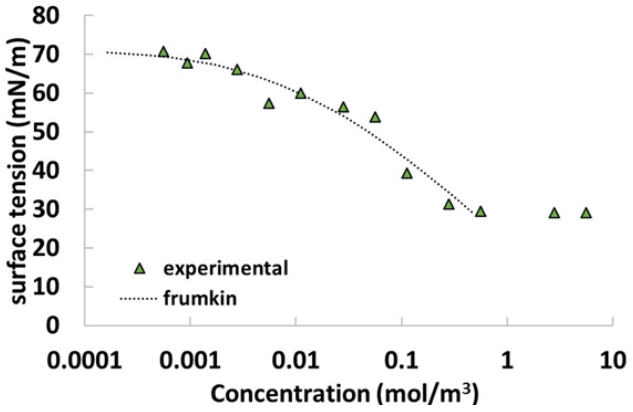

Figure 7. Surface tension of an aqueous mix of surfactant solution as a function of total surfactant concentration.

The curve displays a standard shape, as that of a single surfactant in a solution. The constants obtained are presented in Table 2. Constant a_F was found to be negative, which suggests that the adsorption of surfactants is enhanced by the presence of surfactants in neighboring areas; in other words, adsorption can be attributed to attractive interactions between monomers.

Γ_{∞} (mol.m^{-2})	a_F (-)	K (m^3.mol^{-1})	σ (mN.m^{-1})
2.22×10^{-6}	-1.26	330	42.5

Table 2. Constants of the Frumkin isotherm obtained for an aqueous mix of SDS, SDBS and TX100.

We used the experimental setup of Lebrun et al. (2022b) and the methodology of (Sardeing et al., 2006) to measure mass transfer coefficient in a mix of surfactant solutions with concentrations of 2.8×10^{-6} mol/L, 5×10^{-6} mol/L, and 1×10^{-3} mol/L. According to the Frumkin isotherm, these concentrations lead to an equilibrium coverage ratio of 0.3, 0.4 and 1 respectively. Bubble diameters vary between 4.6 and 5.2 mm, so that equation (24) is used to predict Sherwood numbers. A comparison between experimental Sherwood numbers and those obtained through correlation is presented in Figure 8.

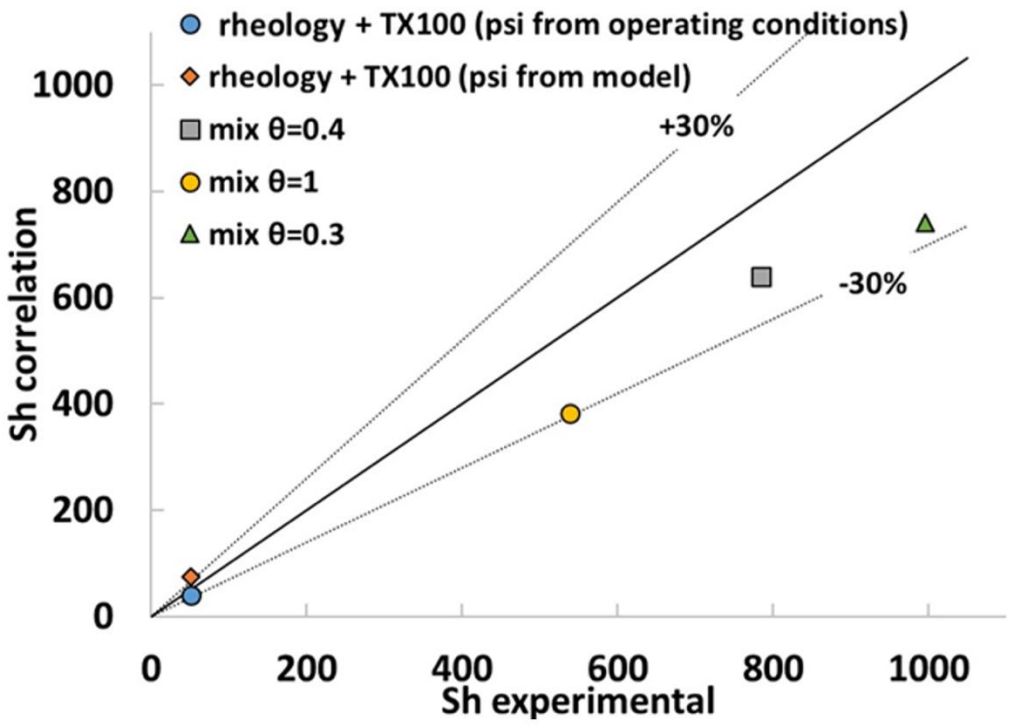

Figure 8. Comparison between experimental Sherwood numbers and those predicted by correlation (24) for a mix of surfactants and correlation (16) for a mix of TX100 and PAAm.

We observed a maximal deviation of 30% for a coverage ratio of 1. Considering the complexity of the liquid phase, the accordance between correlation and experimental values is acceptable. Lebrun et al. (2021) measured oxygen transfer for a bubble of $d_b < 1.5$ mm in water containing a nonionic surfactant (Triton X-100, TX100) and a polymer (polyacrylamide, PAAm); their results are also shown in Figure 8. We compared correlation (24) with the experimental results of this study. The Langmuir constant of TX100 adsorption is taken from Lebrun et al. (2022). The correlation shows a deviation of 20% when the value of

ψ is taken from the operating conditions described in Lebrun et al. (2022b) and 44% if the value is calculated from equation (20). Preliminary applications of the model in complex media (mix of surfactants, non-Newtonian fluid) yield promising results for its potential use in industrial applications, especially in wastewater treatment plants.

Conclusion

This study represents a comprehensive investigation of gas–liquid mass transfer dynamics, specifically focusing on the intricate interplay between surfactants and oxygen transfer in the presence of gas bubbles. Through the examination of more than 300 isolated gas bubbles, our research has yielded a predictive correlation model for oxygen transfer that considers two critical aspects: the hydrodynamic influence of surfactants on mass transfer and the physico-chemical hindrance caused by surfactant adsorption. Recognizing the need for a broader scope of application in wastewater treatment contexts, our study has extended the utility of the model to encompass bubbles with larger Reynolds numbers ($d_b > 1.5$ mm). This effort was facilitated by leveraging the findings of Sardeing et al. (2006), demonstrating its effectiveness in scenarios characterized by the coexistence of multiple surfactant species, which are typical of wastewater treatment plant environments.

Our results underscore the importance of taking into account both hydrodynamic and physico-chemical properties when constructing a predictive mass transfer model. Our model has been rigorously tested and validated for various bubble diameters and surfactant conditions. For smaller bubbles ($d_b < 1.5$ mm), the model exhibits reasonable agreement with experimental data when utilizing a fitted coefficient. For larger bubbles ($d_b > 3.5$ mm), the model attains an even higher degree of accuracy with minimal standard deviation between experimental and predicted Sherwood numbers. In the case of intermediate-sized bubbles ($1.5 \text{ mm} < d_b < 3.5$ mm), further investigation and data collection are required to refine the accuracy of the model.

Furthermore, the applicability of the model has been successfully extended to complex media, including mixtures of surfactants and non-Newtonian fluids. The results obtained in these scenarios hold promise for the practical implementation of the model in industrial applications, particularly in wastewater treatment plants, where oxygen transfer plays a pivotal role in sustaining the microbial activity responsible for

pollutant biodegradation. The present study represents a significant contribution to our understanding of gas–liquid mass transfer dynamics in the presence of surfactants. The predictive correlation model developed herein holds great potential for improving process design and efficiency in wastewater treatment and related industries, while providing a foundation for further research in this critical field of study.

Acknowledgments

The authors wish to thank the French National Research Agency (ANR) for the support received from the project MAMOTHS ANR-17-CE06-001.

References

Alves, S.S., Orvalho, S.P., Vasconcelos, J.M.T., 2005. Effect of bubble contamination on rise velocity and mass transfer. Chemical Engineering Science 60, 1–9. https://doi.org/10.1016/j.ces.2004.07.053

Chen, X., Liu, G., Fan, H., Li, M., Luo, T., Qi, L., Wang, H., 2013. Effects of surfactant contamination on oxygen mass transfer in fine bubble aeration process. Korean Journal of Chemical Engineering 30, 1741–1746. https://doi.org/10.1007/s11814-013-0092-x

Clift, R., Grace, J.R., Weber, M.E., Weber, M.F., 1978. Bubbles, Drops, and Particles. Academic Press.

Dani, A., Cockx, A., Legendre, D., Guiraud, P., 2022. Effect of spheroid bubble interface contamination on gas-liquid mass transfer at intermediate Reynolds numbers: From DNS to Sherwood numbers. Chemical Engineering Science 248, 116979. https://doi.org/10.1016/j.ces.2021.116979

Deising, D., Bothe, D., Marschall, H., 2018. Direct numerical simulation of mass transfer in bubbly flows. Computers & Fluids 172, 524–537. https://doi.org/10.1016/j.compfluid.2018.03.041

García-Abuín, A., Gómez-Díaz, D., Navaza, J.M., Sanjurjo, B., 2010. Effect of surfactant nature upon absorption in a bubble column. Chemical Engineering Science 65, 4484–4490. https://doi.org/10.1016/j.ces.2010.04.009

Gillot, S., Capela-Marsal, S., Roustan, M., Héduit, A., 2005. Predicting oxygen transfer of fine bubble diffused aeration systems—model issued from dimensional analysis. Water Research 39, 1379–1387. https://doi.org/10.1016/j.watres.2005.01.008

Hebrard, G., Zeng, J., Loubiere, K., 2009. Effect of surfactants on liquid side mass transfer coefficients: A new insight. Chemical Engineering Journal 148, 132–138. https://doi.org/10.1016/j.cej.2008.08.027

Jia, X., Hu, W., Yuan, X., Yu, K., 2015. Effect of surfactant type on interfacial area and liquid mass transfer for CO2 absorption in a bubble column. Chinese Journal of Chemical Engineering 23, 476–481. https://doi.org/10.1016/j.cjche.2014.11.027

Jimenez, M., Dietrich, N., Grace, J.R., Hébrard, G., 2014. Oxygen mass transfer and hydrodynamic behaviour in wastewater: Determination of local impact of surfactants by visualization techniques. Water Research 58, 111–121. https://doi.org/10.1016/j.watres.2014.03.065

Kentheswaran, K., Dietrich, N., Tanguy, S., Lalanne, B., 2022. Direct numerical simulation of gas-liquid mass transfer around a spherical contaminated bubble in the stagnant-cap regime. International Journal of Heat and Mass Transfer 198, 123325. https://doi.org/10.1016/j.ijheatmasstransfer.2022.123325

Lebrun, G., Benaissa, S., Le Men, C., Pimienta, V., Hébrard, G., Dietrich, N., 2022a. Effect of surfactant lengths on gas-liquid oxygen mass transfer from a single rising bubble. Chemical Engineering Science 247, 117102. https://doi.org/10.1016/j.ces.2021.117102

Lebrun, G., El Mokdad, B., Le Men, C., Pimienta, V., Coudret, C., Roux, C., Hébrard, G., Dietrich, N., 2022b. Luminescent probe synthesis for oxygen visualization technique: Application to the effect of surfactant structure on oxygen mass transfer. Chemical Engineering Science 260, 117921. https://doi.org/10.1016/j.ces.2022.117921

Lebrun, G., Xu, F., Le Men, C., Hébrard, G., Dietrich, N., 2021. Gas–Liquid Mass Transfer around a Rising Bubble: Combined Effect of Rheology and Surfactant. Fluids 6, 84. https://doi.org/10.3390/fluids6020084

Moore, D.W., 1965. The velocity of rise of distorted gas bubbles in a liquid of small viscosity. Journal of Fluid Mechanics 23, 749–766. https://doi.org/10.1017/S0022112065001660

Orhan, R., Dursun, G., 2016. Effects of surfactants on hydrodynamics and mass transfer in a co-current downflow contacting column. Chemical Engineering Research and Design 109, 477–485. https://doi.org/10.1016/j.cherd.2016.02.030

Pesci, C., Weiner, A., Marschall, H., Bothe, D., 2018. Computational analysis of single rising bubbles influenced by soluble surfactant. Journal of Fluid Mechanics 856, 709–763. https://doi.org/10.1017/jfm.2018.723

Powell, M.J.D., 1964. An efficient method for finding the minimum of a function of several variables without

calculating derivatives. The Computer Journal 7, 155–162. https://doi.org/10.1093/comjnl/7.2.155
Quintero, C.D., 2015. Comportement rhéologique des boues activées : Mesures, modélisation et impact sur le transfert d'oxygène dans les bioréacteurs aérés (phdthesis). INSA de Toulouse.
Rosso, D., Huo, D.L., Stenstrom, M.K., 2006. Effects of interfacial surfactant contamination on bubble gas transfer. Chemical Engineering Science 61, 5500–5514. https://doi.org/10.1016/j.ces.2006.04.018
SA Software [WWW Document], n.d. URL Http://Cinet.Chim.Pagesperso-Orange.Fr/Tele_sa/Install_Sa_Eng.Html.
Sadhal, S.S., Johnson, R.E., 1983. Stokes flow past bubbles and drops partially coated with thin films. Part 1. Stagnant cap of surfactant film – exact solution. Journal of Fluid Mechanics 126, 237–250. https://doi.org/10.1017/S0022112083000130
Sardeing, R., Painmanakul, P., Hébrard, G., 2006. Effect of surfactants on liquid-side mass transfer coefficients in gas–liquid systems: A first step to modeling. Chemical Engineering Science 61, 6249–6260. https://doi.org/10.1016/j.ces.2006.05.051
Takemura, F., 2005. Adsorption of surfactants onto the surface of a spherical rising bubble and its effect on the terminal velocity of the bubble. Physics of Fluids 17, 048104. https://doi.org/10.1063/1.1879712
Tomiyama, A., Celata, G.P., Hosokawa, S., Yoshida, S., 2002. Terminal velocity of single bubbles in surface tension force dominant regime. International Journal of Multiphase Flow 28, 1497.
Weber, M.E., 1975. The effect of surface active agents on mass transfer from spherical cap bubbles. Chemical Engineering Science 30, 1507–1510. https://doi.org/10.1016/0009-2509(75)85028-7
Weiner, A., Timmermann, J., Pesci, C., Grewe, J., Hoffmann, M., Schlüter, M., Bothe, D., 2019. Experimental and numerical investigation of reactive species transport around a small rising bubble. Chemical Engineering Science: X 1, 100007. https://doi.org/10.1016/j.cesx.2019.100007